Int. J. Heat Mass Transfer. Vol. 29, No. 8, pp. 1271–1282, 1986
Printed in Great Britain

0017–9310/86 $3.00 + 0.00
Pergamon Journals Ltd.

Analysis of melting around a moving heat source

M. K. MOALLEMI and R. VISKANTA
Heat Transfer Laboratory, School of Mechanical Engineering, Purdue University, West Lafayette, IN 47907, U.S.A.

Abstract—This paper presents an analysis for simulating melting heat transfer around a moving, horizontal, cylindrical heat source. Motivated by the experimental observations, the melt domain is divided into two regions, namely, the close-contact region and the melt pool region. Two mathematical models are formulated and solution procedures are developed accordingly. The temperature and the flow fields in the two regions are calculated for a constant surface temperature heat source and the resulting velocity of the source and motion and shape of the interface are determined. The effects of the prescribed surface temperature of the source and its density, as well as influence of natural convection in the melt pool, are investigated and reported. The predicted melt flow structure and the motion and shape of the solid–liquid interface are found to be in good agreement with the experimental observations when natural convection in the melt is included in the model.

1. INTRODUCTION

IF A SOURCE releases heat in excess of a certain minimum that its surroundings can conduct, the surroundings will eventually melt and the source will start moving in the melt in the direction of the net forces acting on it (gravitational, buoyancy, shear forces, etc.). This problem arises in nature and technology in such diverse fields as materials processing [1], spacecraft and nuclear technology [2] and geophysics [3]. In the field of nuclear technology, this problem has two important applications. One application is the 'self-burial' process, a nuclear waste disposal scheme which suggests placing the radioactive waste materials in various cavities in the ground [4] or on the arctic ice cap [5]. Another application is the reactor core 'melt-down' process also referred to as the 'China Syndrome' [6, 7].

Phase-change heat transfer problems have been extensively studied during the last decade. The problem considered here, however, has not received proper and adequate attention until recently [8–10]. Emerman and Turcotte [8] have formulated an approximate mathematical model for migration of a hot, rigid sphere which melted its way through a solid. Moallemi and Viskanta [9] have reported experiments with a horizontal, cylindrical heat source which descended in response to gravity while melting the surrounding solid.

In this paper, a mathematical model is formulated for the melting heat transfer problem around a moving heat source. Taking advantage of the experimental observations [9], the melt domain is divided into two regions, and numerical solution procedures are developed for both. The results for a typical set of parameters are presented and general features of the solution are described. The effects of different governing parameters of the problem are also discussed.

2. ANALYSIS

A schematic diagram of the physical problem considered is shown in Fig. 1(a). A horizontal, cylindrical heat source of radius R is initially placed in the solid phase-change material which is at its fusion temperature, T_m. At time $t = 0$, a constant surface temperature T_w is imposed on the surface of the source and the melting begins. The difference between the

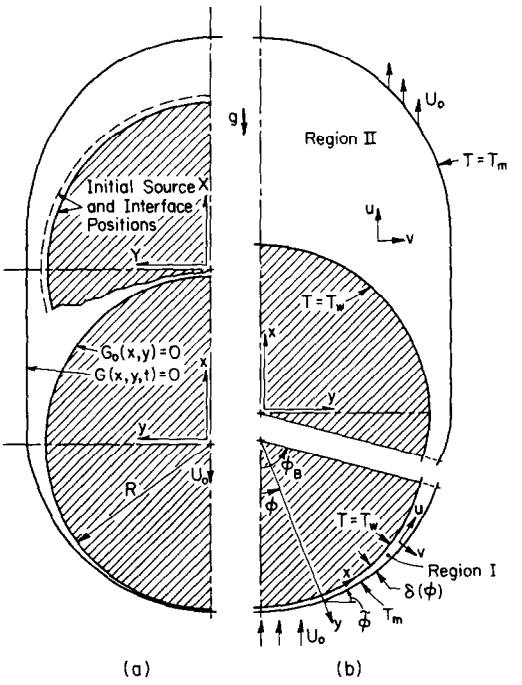

FIG. 1. Schematic diagram of the problem (a) and coordinate systems in regions I and II(b).

NOMENCLATURE

Fo	Fourier number, $\alpha t/R^2$
$G(x, y, t)$	instantaneous interface position function, Fig. 1
$G_0(x, y)$	position function of the surface of the source
g	gravitational constant
h_m	latent heat of fusion
$\mathbf{n}$	unit vector normal to the interface
Pr	Prandtl number, ν/α
p	pressure
q''	heat flux
R	radius of the heat source
Ra	Rayleigh number, $\beta g R^3(T_w - T_m)/\alpha\nu$
Re	local Reynolds number, uR/ν
Ste	Stefan number, $c_p(T_w - T_m)/h_m$
	temperature
t	time
t^*	dimensionless time, Fo^*Ste^*Pr
U_0^*	dimensionless heat source velocity, $U_0 R/\nu$
$\mathbf{u}$	velocity vector with respect to the heat source
(u^*, v^*)	dimensionless velocity components, $uR/\nu, vR/\nu$, Fig. 1
(x^*, y^*)	dimensionless coordinates, $(x, y)/R$, Fig. 1.

Greek symbols

Δ	dimensionless melt layer thickness in region I, δ/R
Δ_0	dimensionless thickness of the melt film at $\phi = 0°$
δ	melt layer thickness in region I
Θ	dimensionless temperature, $(T - T_m)/(T_w - T_m)$
ρ	density
ρ_H	density of the heat source
τ	shear stress
ϕ	circumferential angle, see Fig. 1(b)
$\tilde{\phi}$	interface angle, Fig. 1(b).

Subscripts

B	boundary plane between regions I and II
I	interface
s	solid
w	surface of the heat source.

densities of the source and the melt is assumed to be large enough to produce a continual descent of the source. The solid–liquid interface is assumed to be a sharply defined surface (i.e. melting occurs precisely at T_m). It is also assumed that melt flow is laminar and two-dimensional. The physical properties are assumed to be constant, except for the density in the buoyancy term (Boussinesq approximation).

The problem as posed here has two features that require special treatment in order to obtain realistic results with reasonable cost. First is the fact that the position of solid–liquid interface is not known *a priori* and is to be determined as part of the solution. The second feature which arises from the descent of the source is the fact that the velocity and acceleration of the source are also not known *a priori* and are to be found as part of the overall solution. The experimental observations [9] are employed to formulate a realistic model and to develop a solution procedure for overcoming this difficulty.

The foremost finding of the experimental results is the fact that the physics of the problem divides the melt domain into two distinct and different regions—each with its own scale, transient period and controlling process. Therefore, to take full advantage of the situation, two different sets of assumptions are adapted for the two regions, as shown in Fig. 1(b), and two set of formulations (each with its own solution procedure) are developed. Of these two regions, region I refers to the part of the melt domain under the heat source where $\delta/R \ll 1$, and region II is rest of the melt domain. Experimental results [9] also indicated that the heat source velocity attains its quasi-steady, constant value soon after initiation of melting, and this is assumed to be the case here.

In addition to the general assumption stated earlier and inferred from experimental observations [9], in region I it is assumed that: (1) quasi-steady state is attained with respect to the heat source, or $\partial/\partial t = 0$; (2) the source and the solid are separated by a very thin layer of melt, or $\delta/R \ll 1$; and (3) boundary-layer approximations are valid for the melt flow in the thin film layer. All of the above assumptions are well justified on the basis of the experimental data [9].

With respect to the coordinates systems fixed to the heat source, Fig. 1(b), the governing equations of the problem take the following dimensionless forms (the asterisks denoting dimensionless quantities are dropped for clarity):

$$\frac{\partial u}{\partial x} + \frac{\partial v}{\partial y} = 0 \tag{1}$$

$$Ste\frac{\partial u}{\partial t} + (\mathbf{u}\cdot\nabla)u = -\frac{\partial p}{\partial x} + \frac{\partial^2 u}{\partial x^2} + \frac{\partial^2 u}{\partial y^2} + (Ra/Pr)(g_x/g)\Theta \tag{2}$$

$$Ste\frac{\partial v}{\partial t}+(\mathbf{u}\cdot\nabla)v=-\frac{\partial p}{\partial y}+\frac{\partial^2 v}{\partial x^2}+\frac{\partial^2 v}{\partial y^2}+(Ra/Pr)(g_y/g)\Theta \quad (3)$$

$$Ste\frac{\partial\Theta}{\partial t}+(\mathbf{u}\cdot\nabla)\Theta=\frac{1}{Pr}\left[\frac{\partial^2\Theta}{\partial x^2}+\frac{\partial^2\Theta}{\partial y^2}\right]. \quad (4)$$

In region I the underlined terms are dropped according to the assumptions stated above. To ensure the continuity of the solution, the boundary plane between the two regions, $\phi=\phi_B$, is placed such that the terms eliminated in the formulation of region I are still negligible in region II. Therefore, the formulation of region I is implemented as far as the following criteria are valid:

$$\phi\leqslant\pi/2,\quad \delta(\phi)/R\leqslant 0.1\quad\text{and}\quad u(x,y)\geqslant 0. \quad (5)$$

The boundary conditions in dimensionless form are the following: at the heat source surface ($y=0$ in region I $\sqrt{1-x^2-y^2}=0$ in region II)

$$\mathbf{u}=0\quad\text{and}\quad\Theta=1. \quad (6)$$

At the solid–liquid interface [$y=\Delta(x)$ in region I and $G(x,y,t)=0$ in region II]

$$\mathbf{u}=-\mathbf{U}_0\quad\text{and}\quad\Theta=0 \quad (7)$$

and on the symmetry line ($x=0$)

$$\mathbf{u}=0\quad\text{and}\quad\partial/\partial x=0. \quad (8)$$

No other boundary conditions are required, as the governing equations in region I are parabolic in form (in u and Θ) since the shear stress and heat diffusion along the dominant flow direction x have been neglected. The profiles of the dependent variables and the melt thickness calculated at the boundary plane of the two regions is used by the mathematical model of region II as boundary values. Thus, at $\phi=\phi_B$

$$\mathbf{u}=\mathbf{u}_B\quad\text{and}\quad\Theta=\Theta_B. \quad (9)$$

The energy balance equation at the interface has the following dimensionless form

$$\frac{\partial\Theta}{\partial n}=\left[\frac{\partial G}{\partial t}-\left(\frac{Pr}{Ste}\right)U_0^*\cdot\nabla G\right]\Big/|\nabla G|. \quad (10)$$

In region I, with the interface position $G=y-\Delta(\phi)$, equation (10) reduces to

$$(1+\Delta'^2)\left.\frac{\partial\Theta}{\partial y}\right|_{y=\Delta}=\frac{PrU_0^*}{Ste}\cos\tilde{\phi}. \quad (11)$$

Note that $\phi=x$ due to nondimensionalization, Δ' is $d\Delta/d\phi$, and $\tilde{\phi}$ is the interface angle as shown in Fig. 1(b). The motion of the heat source is governed by Newton's second law of motion and is transformed to

$$\frac{\Delta\rho}{\rho}=\frac{2v^2}{\pi gR^3}\left[\int_0^{\phi_B}(p\cos\phi+\tau_w\sin\phi)\,d\phi+\int_{\phi_B}^{\pi}(p\cos\phi+\tau_w\sin\phi)\,d\phi\right] \quad (12)$$

where $\Delta\rho=\rho_H-\rho$. The integral has been separated into two parts to emphasize the fact that knowledge of the pressure and shear acting on the source in both regions is required in the force balance equation.

3. METHOD OF SOLUTION

The two mathematical models developed for the two regions are coupled not only at the boundary plane of the two regions but also through the source velocity and the force balance equation, equation (12), on the heat source. Since analytical solutions do not appear possible, from the computer memory storage viewpoint, it is desirable to develop a solution procedure such that the two models could be solved one after the other, rather than simultaneously. The model presented for region II requires the profiles of the dependent variables at the boundary plane (as boundary conditions at $\phi=\phi_B$) and the source velocity, which appears in the velocity boundary condition as well as the energy balance equation at the interface. Therefore, region II is solved after the solution for region I has been obtained. To overcome the difficulty of coupling the two models through the force balance equation, the best procedure is to treat the independent parameter $\Delta\rho/\rho$ as a dependent variable to be determined as part of the overall solution. A new independent variable is introduced into the governing equations of region I. The only condition for choosing this new parameter is that it must have a one-to-one relationship with $\Delta\rho/\rho$. From the numerical point of view, the best choice is the melt thickness at the lower stagnation point of the source, Δ_0. Treating Δ_0 as a parameter, U_0^* may be calculated at $\phi=0°$ from equation (11) to yield

$$U_0^*=\left[\left.\frac{\partial\Theta}{\partial y}\right|_{y=\Delta_0}\right]\frac{Ste}{Pr} \quad (13)$$

after setting $\Delta'(0)=0$ and $\tilde{\phi}=0$ due to symmetry. For $\phi>0$, knowing U_0^*, equation (11) is used to determine the melt layer thickness, Δ_0.

With the above change of variables, the model for region I may be solved first and this provides the necessary data (i.e. U_0^* and boundary conditions at $\phi=\phi_B$) for the model in region II. After solving the

model for the two regions, the integrals in the force balance equation, equation (12), are evaluated to yield $\Delta\rho/\rho$. The solution procedures for the two regions are described below.

3.1. *Solution procedures for region I*

The momentum and energy equations in region I, equations (2)–(4), after dropping the underlined terms, are parabolic in form and are solved by a computational scheme which marches along the dominant flow direction x. The numerical marching-integration procedure employed has been successfully applied to close-contact melting with a constant surface heat flux heat source [10, 11] where further details of the method may be found.

3.2. *Solution procedure for region II*

In this region, the model equations (2)–(4) are transient and elliptic in form. The domain—whose boundary changes with time—is irregular and is also part of the solution. To overcome the difficulties associated with the timewise changing melt domain the 'adaptive grid generation' technique [12] is employed. The important advantages of this technique are that: (1) it can conform the shape of the moving solid–liquid interface accurately; and (2) the interior nodes may move adaptively in response to the enlargement of the melt domain and also development of the solution with time. By using a weighting function proportional to $(\nabla\Theta/\Theta)^2$, the grid points are forced to concentrate near the source and the interface where the temperature gradients are largest. The technique is adequately described in the original publication [12] and also in a review article [13]; therefore, only its implementation in the solution procedure is briefly explained here.

The formulation of the solution method is based on control volume approach [14] in general curvilinear coordinates. In the flow field calculations the velocity components are retained in the physical coordinates and a non-staggered grid is employed (i.e. the velocity components and pressure are calculated and stored at the same nodes). This practice eliminates most of the geometric complications as only the fluxes at the faces of the control volume are transformed to the 'imaginary' plane [15], and the geometric coefficients are calculated for only one set of control volumes. However, it makes higher-order interpolations necessary for both the fluxes and the pressure [14] so that stable velocity and pressure fields can be obtained. For flux discretization and interpolation, the 'Flux–Spline' scheme [16] and for pressure interpolation the '$\tilde{P}$–Ω' scheme [17] are used. The solution method along with the adaptive grid generating technique has been successfully applied to a similar problem [10] where further details about the method may be found.

The problem formulation in region II is based on the assumption that the heat source velocity is constant. From the experimental observations [9], this is only true after the boundary layer of the newly melted material is fully established over the heat source. Therefore, the above formulation should be used starting at a time greater than some t_0 and an assumed interface function $G(x, y, t_0)$ such that the above condition is satisfied. As a compromise between accuracy and computational effort, a grid system containing 21×31 nodal points is used. The initial temperature and flow fields assumed are the steady-state solution of the same problem but with a fixed interface (i.e. no melting). The fact that the motion of the interface is slow (compared with the melt velocity in the pool) justifies this choice. The error associated with the choice of initial domain and field is expected to vanish as the melt domain increases in size.

The computational model is based on the assumption that there is a small time lag between the heat transferred to the interface and the interface motion (due to melting and also motion of the heat source). The total dimensionless heat flux at the interface calculated from the temperature and flow field solution at time t is used to determine the interface position at time $t+\Delta t$ from equation (10), with proper spline interpolation to preserve the interface shape. To avoid errors associated with the time lag between heat transferred to the interface and the resultant interface displacement, the computations were started with $\Delta t = 5$ s and the time increment was increased to 10 s at later times into simulation ($\Delta t^* = 0.011$ and 0.022, respectively, for $Ste = 0.0724$). At any time step, the solution was considered converged if

$$\left|\frac{\Phi^{k+1}(i,j)-\Phi^{k}(i,j)}{\max[\Phi^{k+1}(i,j)]}\right| < 10^{-3} \tag{14}$$

where k is the iteration loop counter and Φ is u, v or Θ. Additional details of the solution procedure which is very similar to SIMPLER [14] may be found elsewhere [10].

4. RESULTS AND DISCUSSION

In this section the numerical results for the temperature and velocity fields in the melt in regions I and II are presented. For either of the two regions, first the results for a typical set of parameters are discussed and general features of the problem are described. This is then followed by a discussion of the effects of different governing parameters of the problem; namely, Ste, Ra, Pr, Δ_0 in region I and natural convection in region II.

4.1. *Results in region I*

Representative results in region I were calculated with the following set of parameters: $Ste = 0.0724$, $Ra = 286{,}000$, $Pr = 55.6$ and $\Delta_0 = 0.006$. Figure 2 illustrates the temperature profiles across the melt-

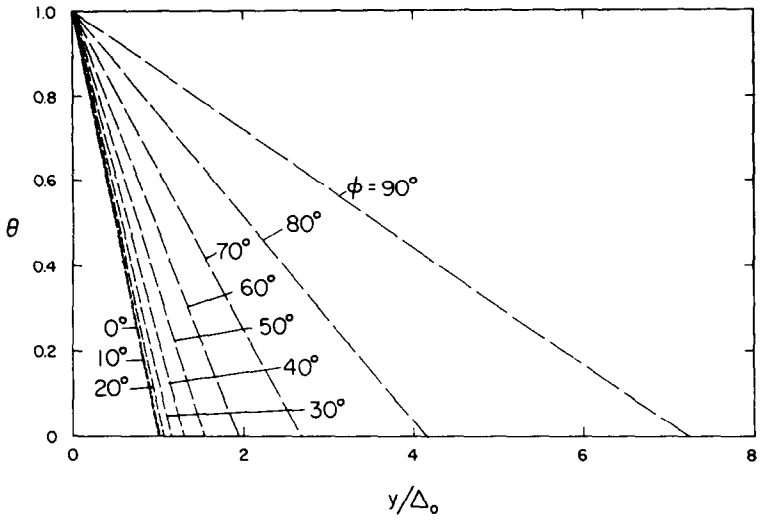

FIG. 2. The melt temperature profiles along the channel.

film at different angular positions along the channel. Close to the lower stagnation point ($\phi = 0°$), the melt-film thickness is very small and the mass flow rate of the melt is also small, thus, melting is due to conduction heat transfer across the melt film and temperature distribution across the melt layer is linear. The growth of the melt-film thickness prevented high melt velocities and heat conduction dominated melting is preserved almost up to 90°. The fact that the Reynolds number (based on the local melt thickness and melt velocity) never exceeded 0.33, for the set of parameters specified, confirms the important role played by conduction along the channel. For the range of parameters examined (i.e. $0.035 \leqslant Ste \leqslant 0.11$, $0.003 \leqslant \Delta_0 \leqslant 0.009$, $0 \leqslant Ra \leqslant 429{,}000$ and $Pr = 55.6$ and 11.0), the maximum deviation of the temperature profiles from a linear temperature distribution never exceeded 5%.

The tangential melt velocity profiles (scaled by the source velocity, U_0) at different angular positions along the melt channel are presented in Fig. 3. The first point to note in the figure is the way the tangential melt velocity develops along the film channel (i.e. the local maximum velocity increases first and then decreases, with absolute maximum of 126 U_0^* occurring at $\phi = 46.1°$). This may be explained by simultaneous consideration of the rate of growth of the melt-film thickness and the entrainment rate of the melt into the channel.

The normal melt velocity at the solid–liquid interface is a measure of the entrainment and decreases with ϕ [it is proportional to $\cos\phi$, equation (7)]. Near

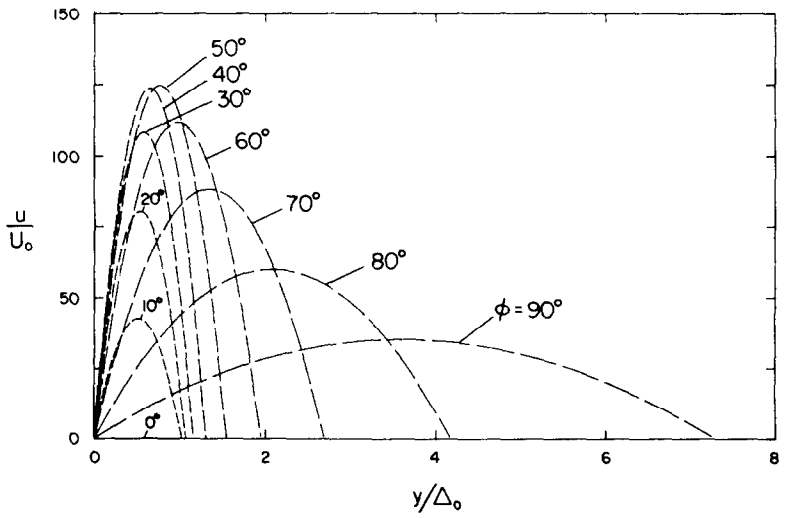

FIG. 3. The tangential velocity profiles of the melt along the channel.

$\phi = 0°$, the entrainment of the melt is high enough to compensate for the widening of the melt film and also to cause an increase in the tangential melt velocity. Whereas, further along the channel, the rate of growth of the melt film becomes large enough not only to compensate for entraining melt but also to decelerate the melt flow. For the range of parameters examined, the location of the maximum average melt velocity was found to be between 44.7° and 47.3°, which is in good agreement with $\phi = 45°$ predicted by the approximate model [9, 10].

Table 1 presents the dimensionless parameters and summary of the results of the numerical simulations with different values of Δ_0 and *Ste*, *Ra* and *Pr*. First *n*-octadecane is chosen as the phase-change material ($Pr = 55.6$). For all the cases examined, the marching-integration was performed up to $\phi_B = 90°$ as neither of the last two criteria of equation (5) was violated (i.e. melt layer thickness remained less than 10% of the radius of the source and no flow recirculation occurred up to $\phi = 90°$).

The values of pressure at $\phi = \phi_B$ [with respect to $p(0°) = 0$] and the first integral in equation (12) are calculated in region I and are used in calculations for region II in order to determine $\Delta\rho/\rho$. To compare the numerical results with the approximate solution [9, 10], the value of $\Delta\rho/\rho$ may be calculated by assuming that $p(\phi) = p(\phi_B)$ and $\tau_w(\phi) = 0$ for $\phi_B \leqslant \phi \leqslant \pi$ which is also assumed in deriving the approximate solution [9, 10]. With these assumptions and for different values of Δ_0 and *Ste*, the effective densities of the heat source are calculated and are presented in Table 1. The calculated values of $\Delta\rho/\rho$ fall between the approximate analytical predictions and experimental results [9, 10] (i.e. 6–16% higher than predictions and 10–15% lower than measurements). The difference may be attributed to the simplification of the approximate model and also the idealizations of the experiments.

The angular variation of Δ/Δ_0 calculated by the numerical scheme for different values of *Ste* and Δ_0 is presented in Fig. 4. The figure shows that most of growth in the melt film thickness takes place in the last 15° of the channel. Up to $\phi \approx 50°$, the dependence of $\Delta(\phi)$ on *Ste* and $\Delta\rho/\rho$ remains exactly the same as that of Δ_0 as Δ/Δ_0 is independent of *Ste* for all Δ_0s. For this part of the melt channel, the ratio of the heat fluxes $q''_w(\phi)/q''_{w0}$ at the surface of the source at ϕ and 0°, respectively, is also independent of *Ste* and Δ_0. For ϕs larger than 50° the effect of Δ_0 on Δ/Δ_0 and q''_w/q''_{w0} gradually becomes evident, but Δ_0 and q''_{w0} still carry the influence of *Ste* and $\Delta\rho/\rho$ (i.e. identical results for $Ste = 0.0358$, 0.0724 and 0.11). The bulk average temperature of the melt was calculated along the channel and found to be constant (at least for $0 \leqslant \phi \leqslant 80°$) and close to the mean temperature, $\Theta = 0.5$. This finding confirms the relatively minor role played by convection compared to conduction heat transfer. The maximum Reynolds numbers which always occurred at $\phi = 90°$ are presented for different runs presented in Table 1 and are all less than unity (Péclet number less than 55), which again confirms the small effect of convection heat transfer in the channel.

Table 1 also illustrates the effects of the buoyancy force on the solution. This can be done by comparing the results for $Ra = 286{,}000$ with those in which $Ra = 0$. The heat source velocity is defined $\phi = 0°$ and is essentially governed by conduction heat transfer between the source and the solid; therefore, it is not affected by the neglect of the buoyancy force in the

Table 1. Dimensionless parameters and results for different values of *Ste*, Δ_0, *Ra* and *Pr*

Variable changed	Δ_0	*Ste*	*Ra*	*Pr*	U_0†	ϕ_B	$\Delta(\phi_B)$	$P(\phi_B)$	q''_l/q''_w	Re_{max}†	$\Delta\rho/\rho$‡
Δ_0	0.003	0.0724	286,000	55.6	0.4234	90°	0.02712	-4.78×10^7	0.9654	0.6465	20.45
	0.006§	0.0724	286,000	55.6	0.2117	90°	0.04343	-3.03×10^6	0.9651	0.3260	1.305
	0.009	0.0724	286,000	55.6	0.1411	90°	0.05724	-9.03×10^5	0.9645	0.2191	0.2616
Ste	0.006	0.0358	143,000	55.6	0.1060	90°	0.04342	-1.52×10^6	0.9824	0.1633	0.6534
	0.006§	0.0724	286,000	55.6	0.2117	90°	0.04343	-3.03×10^6	0.9651	0.3260	1.305
	0.006	0.0110	429,000	55.6	0.3177	90°	0.04342	-4.54×10^6	0.9482	0.4893	1.958
Ra	0.006	0.0724	0	55.6	0.2117	90°	0.04360	-3.07×10^6	0.9677	0.3284	1.313
	0.006§	0.0724	286,000	55.6	0.2117	90°	0.04343	-3.03×10^6	0.9651	0.3260	1.305
Pr‖	0.006	0.0504	18,800	11.0	0.7505	90°	0.04345	-1.07×10^7	0.9758	1.156	0.3788
	0.006	0.0358	143,000	55.6	0.1060	90°	0.04342	-1.52×10^6	0.9824	0.1633	0.6534

† $Re_{max} = U_{max}(\phi_B)\Delta(\phi_B)$.
‡ Calculated with the assumption that $p(\phi) = p(\phi_B)$ and $\tau_w(\phi) = 0$ for $\phi_B \leqslant \phi \leqslant 180°$.
§ Standard case.
‖ Results for water and *n*-octadecane, both with $T_w - T_m = 4°C$.

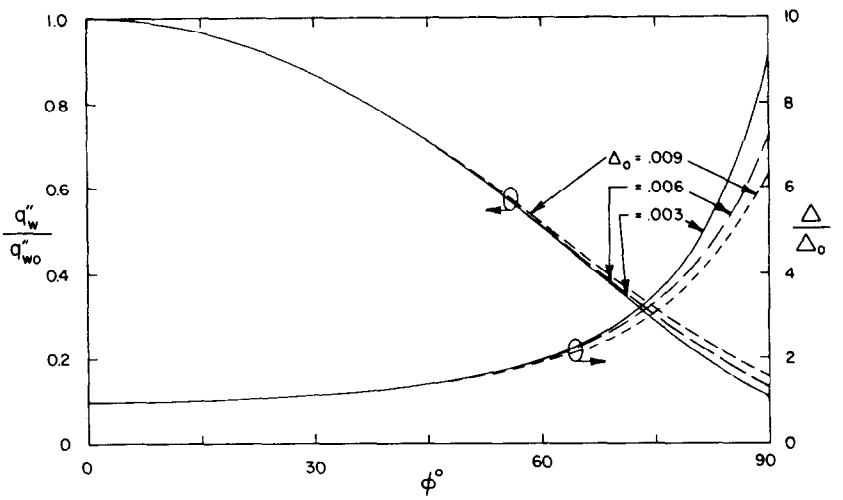

FIG. 4. Angular variation of Δ/Δ_0 and q''_w/q''_{w0} for $Ste = 0.0358$, 0.0724 and 0.110.

melt. Overall the effect of buoyancy in the melt is concluded to be negligible as the melt layer thickness increased by less than 0.4% at 90° and the effective density of the source increased by about 0.6% when Ra was set to zero.

The general features of the problem in this region did not change when ice ($Pr = 11.0$) was used as phase-change material instead of n-octadecane. The results of two computer simulations, both with $T_w - T_m = 4°C$, for these two phase-change materials are compared in Table 1. An examination of the results reveals that the solutions are very similar and the calculated value of $\Delta\rho/\rho$ is about 11% greater than that predicted by the approximate solution [9, 11].

4.2. *Results for region II*

The representative results in region II were calculated for the standard set of parameters ($Ste = 0.0724$, $Ra = 286{,}000$, $\Delta_0 = 0.006$ and $Pr = 55.6$) and an assumed initial melt pool as shown in Fig. 5 with the melt layer thickness and the profiles of the dependent variables at $\phi = \phi_B$ taken from the solution of the problem in region I for the same set of model parameters. The initial velocity and temperature fields are also presented in Fig. 5 in the form of streamline and isotherm contours.

Figure 6 presents the temperature and the velocity distributions in the melt at four different times in the course of the numerical simulation. The predictions are in excellent qualitative agreement with the experimental results [9, 10]. The melt entering the computational domain, at the boundary plane $\phi = \phi_B$, forms a boundary layer along the surface of the source. This boundary layer and the one formed by the cooled melt along the interface are separated by a nearly stagnant core of isothermal melt. By comparing the flow and temperature fields in Figs. 6(c) and (d), it can be seen that the quasi-steady state had already been established in the vicinity of the source (with respect to the source). Continued melting only results in growth (elongation) of the stagnant core (due to descent of the source as well as motion of the interface)

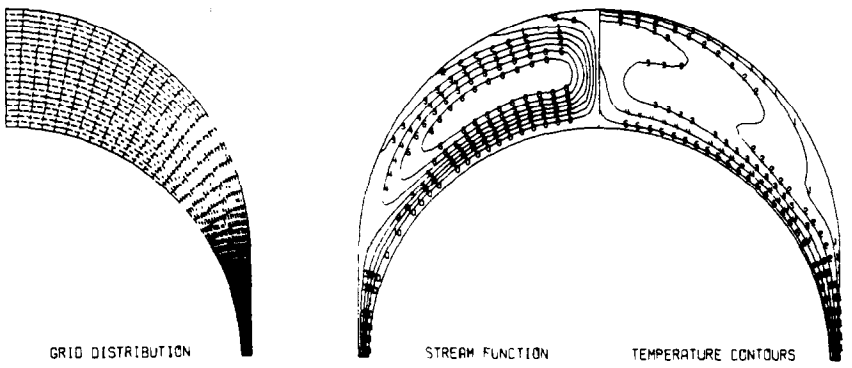

FIG. 5. Initial grid distribution, flow and temperature field.

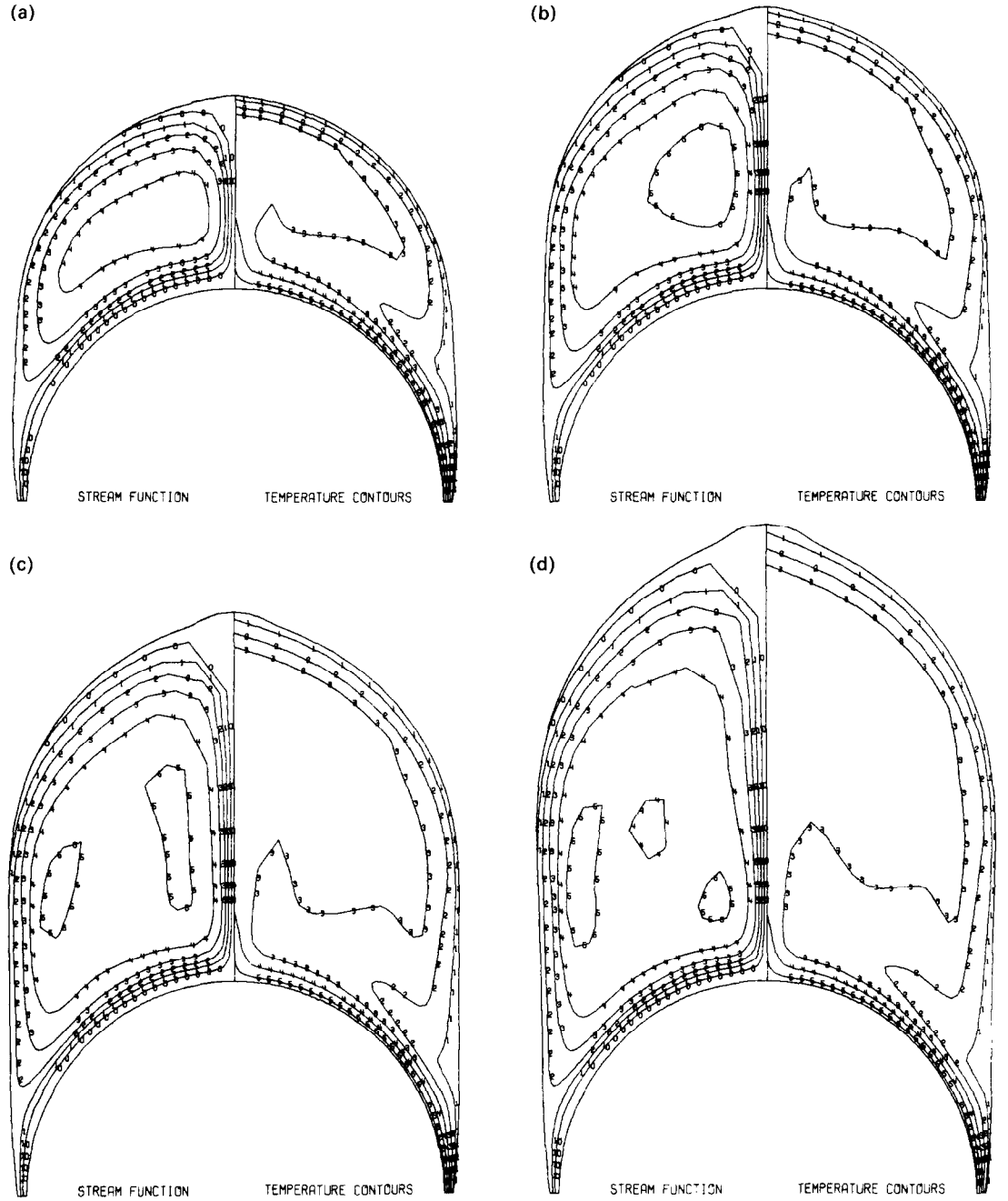

FIG. 6. Flow pattern and temperature distributions at different times, $t^* = 0.135$ (a); 0.269 (b); 0.404 (c); and 0.539 (d) for $Ste = 0.0724$ and $Ra = 286{,}000$.

and does not affect the boundary layer along the surface of the source. Examination of temporal variation of the angular variation of the heat transfer coefficient at the surface of the source revealed that the quasi-steady state has been reached over the heat source by $t^* = 0.404$, which corresponds to the flow field presented in Fig. 6(c) [10].

Figure 7 shows the interface position at the beginning (assumed) and also at selected times into the simulation. The gradual evolvement of the interface towards its quasi-steady state shape with respect to the source is illustrated in the figure. Due to the fact that the solid is not subcooled, the entire interface is not expected to attain a quasi-steady-state shape. However, after 180 s into the simulation ($t^* = 0.404$), the interface in the vicinity of the source (at least up to $\phi = 120°$) had already reached its quasi-steady-state shape. The calculated interface shape is in good

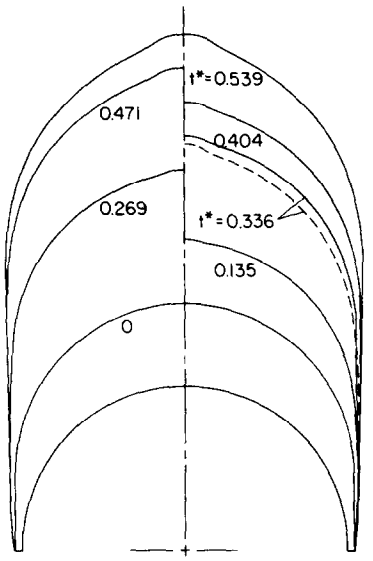

FIG. 7. Solid–liquid interface positions with respect to the source at different times for $Ste = 0.0724$, $Ra = 286{,}000$ (solid lines) and $Ra = 0$ (dashed line).

general agreement with the experimental observations [9, 10]. Extensive and localized melting around $\phi = 180°$ is common in both the experimental observations [9, 10]. For the case of the stationary source, similar non-symmetric melting around the upper stagnation point has also been observed [18, 19] which eventually resulted in formation of a 'pear-like' shaped solid–liquid interface. For a descending heat source, however, the extensive localized melting around $\phi = 180°$ which is clearly present at early times in the simulation does not seem to persist with time. The upward motion of the interface in the present study (due to the descent of the source) reduces the intensity of the interaction between the plume and the interface. Examination of the variation of the heat flux along the interface revealed that the position of maximum heat transfer coefficient changes with descent of the source and is not fixed at 180° as has been reported to be the case for the stationary source cases [18, 19].

The effects of natural convection on the flow structure in the melt pool as well as the motion of the interface were investigated by setting $Ra = 0$ deliberately, while keeping all the other parameters the same as in the standard case. The initial melt domain was chosen as shown in Fig. 5, and the initial flow field is displayed in Fig. 8(a). The streamlines and isotherms at three selected times into the simulation are also presented in Figs. 8(b)–(d). These figures show that neglect of the buoyancy effects eliminates the driving force for melt recirculation and results in the disappearance of the stagnant, isothermal melt core. With no flow recirculation to comply with the velocity boundary condition at the interface, the streamlines diverge while entering the melt pool. No boundary layer is formed over the source nor along the interface, and the melt flow closely resembles flow over a cylinder in an infinite medium for $Re < 10$ [20]. Absence of the boundary layer over the heat source results in large reduction in the heat transfer from the source (e.g. 42% reduction in $\overline{Nu}_w$) compared to the standard case.

At the interface, however, neglect of natural convection in the melt results in an increase in the heat transfer to the interface near the source, while causing a decrease away from the source. The effect of this variation in heat transfer to the interface on its motion is illustrated in Fig. 7 where the interface positions at $t^* = 0.336$ for $Ste = 0.0724$ are compared for the two values of Ra. This figure indicates that the indirect (convective) melting would be greatly underestimated if natural convection in the melt is not considered [note that the volume of the directly melted material (by conduction) is the same for both cases as U_0^* does not change by setting $Ra = 0$, Table 1]. Therefore, it is concluded that natural convection is important (and should be included) in predicting flow structure in the melt pool as well as the interface motion.

A melting simulation has been performed for $Ste = 0.0358$, and the results are compared with the standard case (with $Ste = 0.0724$) to examine the effect of the surface temperature of the source on the flow pattern in the melt pool as well as the interface motion. The melt flow structure [10] is found to be similar to the base case, although melt recirculation is weaker here due to smaller Rayleigh number (i.e. $Ra = 143{,}000$ in this case compared to 286,000 for the base case).

The pressure field in the melt pool was calculated as a part of the solution in region II. Comparison of the dimensionless pressure difference in the melt layer in region I (Table 1) shows that the pressure field in region II is quite uniform ($\Delta p_{max} = 7.0 \times 10^3$ in region II compared with $\Delta p = 3.03 \times 10^6$ in region I). From the calculated velocity and pressure field in region II, the relative density of the source $\Delta\rho/\rho$ was determined to be equal to 1.2996 after integration of equation (12). In Table 1, for the same set of parameters but with the assumptions that in region II pressure is constant and shear force on the surface of the source is negligible, $\Delta\rho/\rho$ was calculated to be equal to 1.305. These assumptions cause only 0.4% error in the estimate of $\Delta\rho/\rho$ and are thus well justified.

The sensitivity of the solution to the initially assumed interface was examined in a simulation with a differential melt domain (i.e. 100% increase in melt pool height at $\phi = 180°$). A comparison of the temperature and flow fields calculated in this simulation, with those of the standard case [Figs. 8(c) and (d)] has revealed that the difference in the flow development is very small and is mostly confined to the stagnant, isothermal melt core. The maximum difference in the quasi-steady-state values of Nu_w is less than 7% and occurs at $\approx 150°$. The quasi-steady-state shapes of the interface in the immediate vicinity of the source are the same for the two cases [10].

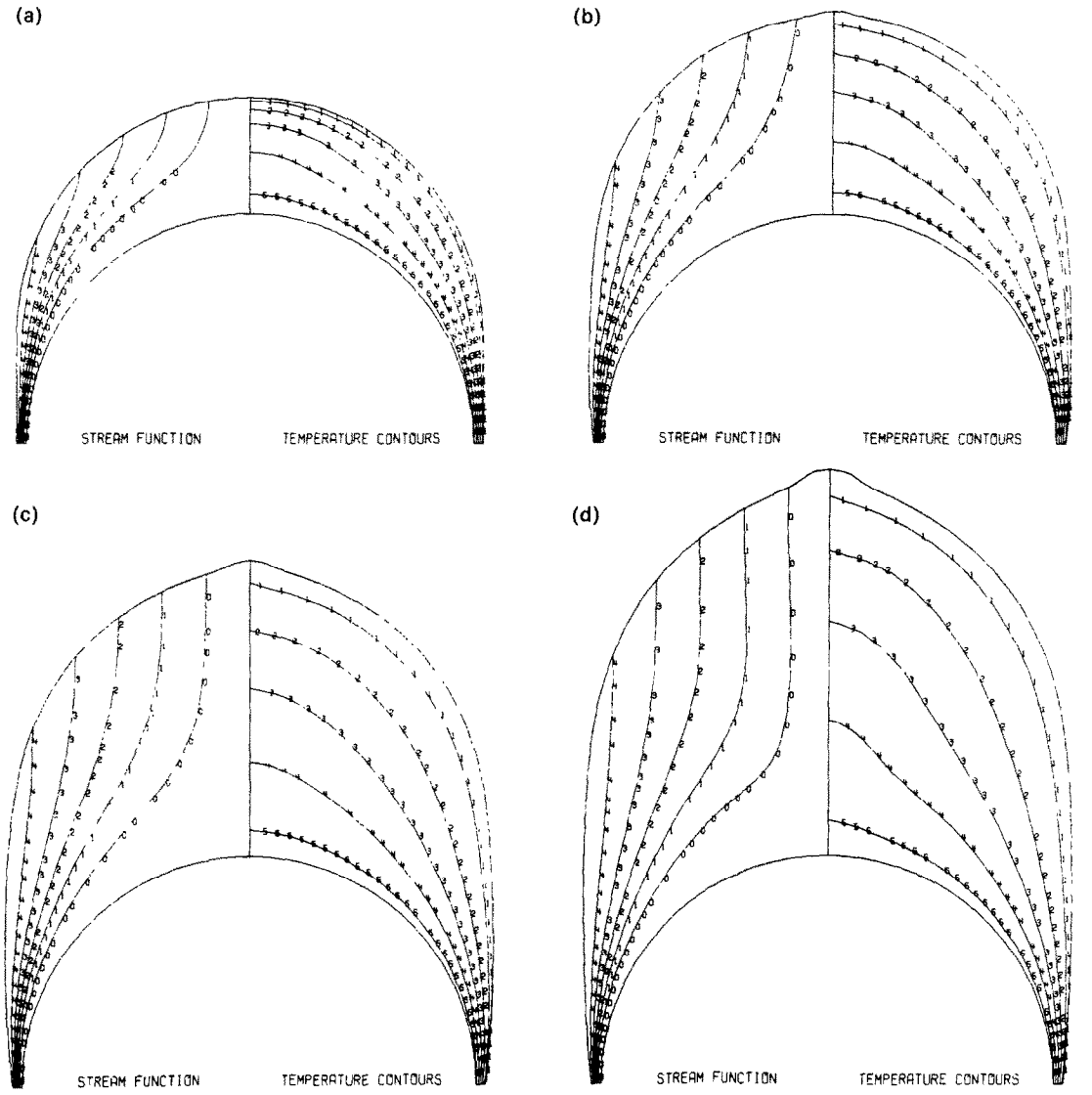

FIG. 8. Flow pattern and temperature distribution at different times for $Ste = 0.0724$ and $Ra = 0$: $t^* = 0.0$ (a); 0.135 (b); 0.269 (c); and 0.404 (d).

5. CONCLUSIONS

An analysis has been developed to predict melting heat transfer around a migrating heat source by dividing the melt domain into two regions. Region I is the melt domain under the source where the melt layer thickness is very small and no recirculation takes place. In this region, the problem is governed by a set of parabolic equations. Region II occupies the rest of the melt domain where melt recirculation may take place and thus the governing equations are of the elliptic type. The results of numerical simulations were found to be in good agreement with the experimental observations, and thus justified the division of the melt into two regions.

In region I, conduction was found to be the dominant mode of heat transfer between the source and the solid. The numerical results for region II indicated that the pressure and shear forces acting on the surface of the source in this region are essentially uniform. This suggests that the solution of the problem in region I is sufficient to determine the velocity of the source as a function of the Stefan number and the relative density of the source.

The calculated flow and temperature fields in region II were found to be in good qualitative agreement with the experimental observations. The melt flow in the wake of the source consisted of two boundary layers, one stretched over the heat source and the other along the solid–liquid interface. The formation of these boundary layers was found to be a result of circulation by natural convection of the melt in the

melt pool above the heat source. The boundary-layer formation over the source isolated the source from the melt pool and interface away from it. As a result, the source and the solid–liquid interface in its immediate vicinity reached their quasi-steady state not later than the time that boundary-layer formation of the newly melted material was completed on and over the source.

Acknowledgements—The work described in this paper was partially supported by the National Science Foundation Heat Transfer Program under Grant No. MEA-8313573. The authors would like to acknowledge helpful discussions with Dr A. Ungan concerning the implementation of the adaptive grid generating algorithm. Computer facilities were made available by Purdue University Computer Center.

REFERENCES

1. F. Jackson, Moving heat sources with change of phase, *J. Heat Transfer* **87,** 329–332 (1965).
2. L. S. Tong, Core cooling in a hypothetical loss of coolant accident. Estimate of heat transfer in core meltdown, *Nucl. Engng Des.* **88,** 309–312 (1968).
3. B. D. Marsh, On the cooling of ascending andesitic magma, *Phil. Trans. R. Soc.* **A288,** 611–625 (1978).
4. J. J. Cohen, L. L. Schwartz and H. A. Tewes, Economic and environment evaluation of nuclear waste disposal by underground in situ melting, *Am. Nucl. Soc. Trans.* **18,** 194–195 (1974).
5. A. G. Herrmann, *Radioaktive Abfalle*. Springer, Berlin (1983).
6. G. Jansen and D. D. Stepnewski, Fast reactor fuel interactions with floor material after a hypothetical core meltdown, *Nucl. Technol.* **17,** 85–96 (1973).
7. N. C. Rasmussen, J. Yellin, D. J. Kleitman and R. B. Stewart, Nuclear power: can we live with it?, *Technol. Rev.* **81,** 32–46 (1979).
8. S. H. Emerman and D. L. Turcotte, Stokes' problem with melting, *Int. J. Heat Mass Transfer* **26,** 1625–1630 (1983).
9. M. K. Moallemi and R. Viskanta, Melting heat transfer around a migrating heat source. *J. Heat Transfer* **107,** 451–458 (1985).
10. M. K. Moallemi, Melting around a migrating heat source. Ph.D. thesis, Purdue University, West Lafayette, IN (1985).
11. M. K. Moallemi and R. Viskanta, Analysis of close-contact melting heat transfer, *Int. J. Heat Mass Transfer* **29,** 855–867 (1986).
12. J. U. Brackbill and J. S. Saltzman, Adaptive zoning for singular problems in two dimensions, *J. comp. Phys.* **46,** 342–368 (1982).
13. J. F. Thompson, A survey of grid generation techniques in computational fluid dynamics, AIAA Paper No. 83-0447 (1983).
14. S. V. Patankar, *Numerical Heat Transfer and Fluid Flow*. Hemisphere, Washington, DC (1980).
15. S. P. Vanka, B. C. Chen and W. T. Sha, Semi-implicit calculation procedure for flows described in boundary-fitted coordinate systems, *Numer. Heat Transfer* **3,** 1–19 (1980).
16. L. M. C. Varejao, Flux-spline method for heat, mass, and momentum transfer. Ph.D. thesis, University of Minnesota, Minneapolis, MN (1979).
17. C. F. Hsu, A curvilinear-coordinate method for momentum, heat and mass transfer in domains of irregular geometry. Ph.D. thesis, University of Minnesota, Minneapolis, MN (1981).
18. A. G. Bathelt, R. Viskanta and W. Leidenfrost, An experimental investigation of natural convection in the melted region around a heated horizontal cylinder, *J. Fluid Mech.* **90,** 227–239 (1979).
19. H. Reiger, U. Projahn and H. Beer, Analysis of the heat transport mechanisms during melting around a horizontal circular cylinder, *Int. J. Heat Mass Transfer* **25,** 137–147 (1982).
20. H. Schlichting, *Boundary Layer Theory*, 7th edn. McGraw-Hill, New York (1979).

ANALYSE DE LA FUSION D'UNE SOURCE DE CHALEUR MOBILE

Résumé—On présente une analyse de simulation de la fusion autour d'une source de chaleur mobile horizontale et cylindrique. A partir des observations expérimentales, le domaine de fusion est divisé en deux régions, celle de contact direct et celle du bain fondu. Deux modèles mathématiques sont formulés et des procédures de résolution développées. Les champs de température et de vitesse dans les deux régions sont calculés pour une température constante de la source et la vitesse résultante de la source, le mouvement et la forme de l'interface sont déterminés. On s'intéresse aux effets de la température de surface prescrite et de la densité de la source aussi bien qu'à l'influence de la convection naturelle dans le bain fondu. La structure de l'écoulement, le mouvement et la forme de l'interface solide–liquide déterminés par le calcul sont en bon accord avec les observations expérimentales quand la convection naturelle dans le bain de fusion est incluse dans le modèle.

STUDIE ÜBER DAS SCHMELZEN AN EINER SICH BEWEGENDEN WÄRMEQUELLE

Zusammenfassung—Dieser Beitrag stellt eine Studie zur Simulierung des Wärmeübergangs beim Schmelzen an einer sich bewegenden horizontalen, zylindrischen Wärmequelle vor. Beobachtungen beim Experiment zeigten, daß das Schmelzgebiet in zwei Bereiche eingeteilt werden kann, nämlich in das wärmequellennehe Gebiet und das Gebiet des Schmelzbades. Es werden zwei mathematische Modelle aufgestellt und die entsprechenden Lösungsverfahren angegeben. Das Temperatur- und das Strömungsfeld in den beiden Gebieten werden für eine konstante Oberflächentemperatur der Wärmequelle berechnet, die resultierende Geschwindigkeit der Wärmequelle und die Bewegung und Gestalt der Grenzfläche werden bestimmt. Die Effekte, die durch die aufgeprägte Oberflächentemperatur der Quelle und seine Dichte entstehen, sowie der Einfluß der natürlichen Konvektion im Schmelzbad werden untersucht und dargestellt. Der berechnete Schmelzablauf und die Bewegung und Gestalt der Grenzfläche zwischen fester und flüssiger Phase stimmen gut mit den Beobachtungen bei Experimenten überein, wenn die natürliche Konvektion in der Schmelze im Modell berücksichtigt wird.

АНАЛИЗ ПЛАВЛЕНИЯ ОКОЛО ДВИЖУЩЕГОСЯ ИСТОЧНИКА ТЕПЛА

Аннотация—Проведено моделирование теплопереноса при плавлении около движущегося горизонтального, цилиндрического источника тепла. Эксперименты показали, что область плавления разделена на две части: зону непосредственного контакта и зону большого объема расплава. Сформулированы две математические модели, для которых разработаны методы решения. Поля температуры и течения в обеих зонах рассчитаны для постоянной температуры поверхности источника тепла и его результирующей скорости; определены скорость движения и форма границы между зонами. Исследовано влияние заданной температуры поверхности источника и его интенсивности, а также естественной конвекции в объеме расплава. Найдено, что рассчитанная структура течения расплава, а также форма и характер движения раздела твердое тело жидкость хорошо согласуются с экспериментом при учете естественной конвекции в расплаве.